RSC Sustainability

ROYAL SOCIETY OF CHEMISTRY

PAPER

View Article Online
View Journal | View Issue

Cite this: *RSC Sustainability*, 2024, **2**, 1599

Sustainable synthesis of carbon dots from *Ananas Comosus* as renewable biomass: nanomolar level detection of glutathione†

Mallika Phull, Amjad Ali and Banibrata Maity *

The adoption of green alternatives has become critically important for ensuring a sustainable environment in light of the state of our ecosystem. Biomass, being carbon-rich and environmentally benign, has garnered significant attention and has emerged as a viable solution. Herein, we report the synthesis of highly fluorescent intrinsic nitrogen-functionalized carbon dots using *Ananas Comosus* (AC-CQDs) juice as a renewable biomass precursor through a microwave-aided pyrolysis method utilizing only its natural ingredients. This approach was executed without the use of any chemical additive, underscoring its applicability as a green methodology. Besides, the as-prepared AC-CQDs exhibited high biocompatibility, water solubility, and photostability, and the synthesis protocol was also facile and cost effective. The surface state functionalization and nature of the synthesized AC-CQDs were characterized and confirmed by X-ray photoelectron spectroscopy, X-ray diffraction, and Fourier transform-infrared and Raman spectroscopic analyses. The average size of the AC-CQDs was observed to be 2.25 nm *via* HR-TEM analysis. In order to ensure the stability of the AC-CQDs, the impact of pH variation, irradiation time, ionic strength, and storage duration were investigated. The as-prepared nanoprobe displayed a substantial PLQY value of ~48% and, further, showed high selectivity and sensitivity for the label-free determination of Mn(VII) ions. The interaction of the synthesized AC-CQDs with Mn(VII) ions showed promising fluorescence turn-off quenching, and the sensitivity of AC-CQDs toward Mn(VII) ions was found to be up to the nanomolar range with a limit of detection of 14 nM. Furthermore, fluorescence restoration of the proposed nanosensor [AC-CQDs@Mn(VII)] was observed by the addition of glutathione (GSH). This fluorescence turn-on–off–on nanoprobe showed an appreciable detection limit up to the nanomolar range (8.8 nM) for GSH with a satisfactory linearity range between 0 and 250 nM. Various photophysical parameters of the AC-CQDs were thoroughly investigated in the presence of dual analytes to acquire a better understanding of the sensing mechanism. For ensuring the high precision of the dual analytes in the proposed nanosensor, a number of analytical parameters were also examined. In addition to this, the feasibility of the designed nanosensor was assessed through paper strip testing, and to gauge the viability of the detection approach, real sample analysis was undertaken, showcasing satisfactory recovery rates and relative standard deviations with respect to the developed probe. This study aligns well with the UN's Sustainable Development Goal 3 (good health and well-being) and 12 (responsible consumption and production). Thus, the nanosensor derived from biomass precursors will pave a path for the development of CQDs through a straightforward, swift, cost-effective and green approach.

Received 8th January 2024
Accepted 12th April 2024

DOI: 10.1039/d4su00004h

rsc.li/rscsus

Sustainability spotlight

Glutathione (GSH) is a tripeptide produced by the liver in the human body and is involved in several processes, such as DNA repair, tissue building and the generation of chemicals and proteins. Deviations from the normal levels of GSH can result in several neurodegenerative disorders such as Alzheimer's and Parkinson's and cancer. Therefore, the detection of GSH is of critical relevance. Herein, we report a facile, green, and cost-effective approach involving biomass (*Ananas Comosus*)-derived carbon dots with a limit of detection of 8.8 nM, which is even lower than that obtained by commercially available GSH assay kits (Sigma). Furthermore, this work aligns well with the UN's SD Goals 3 (good health and well-being) and 12 (responsible consumption and production) owing to the sharp decline in the availability of non-renewable resources.

School of Chemistry and Biochemistry, Thapar Institute of Engineering and Technology, Patiala 147004, India. E-mail: banibrata.maity@thapar.edu; phullmallika96@gmail.com; amjadali@thapar.edu

† Electronic supplementary information (ESI) available. See DOI: https://doi.org/10.1039/d4su00004h

1. Introduction

Glutathione (GSH) is a tripeptide composed of three amino acids: cysteine, glutamic acid, and glycine.[1] Mammalian liver tissues contain this non-protein thiol (GSH), which ranges in size from 5 to 10 mM in both oxidized and reduced states. GSH is an important antioxidant that aids in the neutralization of reactive oxygen species, thus acting as a radical scavenger.[2] It also helps in the transportation of amino acids and maintains the formation of disulfide bonds in proteins.[3] GSH also assists in a variety of other biological processes, such as detoxification, metabolism, gene regulation, redox homeostasis, and signal transduction.[4] The abnormal levels of GSH can cause various diseases, including cystic fibrosis, neurodegenerative diseases such as Alzheimer's[5] and Parkinson's, AIDS, diabetes, aging,[6] and cancer.[7] In light of its aforementioned biomedical significance, the measurement and sensitive detection of GSH has garnered immense attention over the past few decades. To date, several analytical methods for the detection of GSH have been proposed, including capillary electrophoresis,[8] surface-enhanced Raman scattering,[9] high-performance liquid chromatography,[10] mass spectroscopy, enzyme-linked immunosorbent assay,[11] and UV-vis assays. However, all of these procedures are time-consuming, with low sensitivity, and require expensive equipment, thus significantly reducing their practical utility. A more advantageous option is fluorescence spectroscopy, which is a simple and highly sensitive approach.[12] Fluorescence-based sensors have numerous advantages, including a rapid response mechanism, high selectivity, and simple functioning. Recently, Shao *et al.* reported a fluorescence sensor for the detection of GSH using bis-spiropyran ligands.[13] Prior to this, a number of organic dyes were extensively used as fluorescent probes, but their narrow excitation spectra, poor photostability, and tailing of the emission band limited their application.[14] As a result, various fluorescent nanomaterials with excellent fluorescence characteristics emerged to circumvent these constraints. Nanomaterials, such as graphene oxide (GO),[15] carbon dots, gold nanoparticles,[16,17] graphitic carbon nitride (g-CNQD),[18] and upconversion nanoparticles (UCNPs),[19] have been widely reported for the detection of GSH.

The synthesis of fluorescent materials from biomass has emerged as an excellent alternative due to the increasing demand but sharp decline in the availability of non-renewable resources. Biomass is an abundant heterogeneous, organic, and biodegradable composite. Biomass wastes can be derived from agriculture, forestry, domestic garbage fishery, *etc.*[20] Besides, being a rich source of carbon, biomass is enriched with proteins and ash and is composed of cellulose and lignin.

Zero-dimensional (0D) carbon dots obtained from biomass have intriguing properties, like biocompatibility, high chemical stability, low toxicity, and wavelength tunable emission properties. Carbon dots can be synthesized using a variety of approaches, including ultrasonication, solvothermal methods, microwave treatment, chemical oxidation, hydrothermal treatment, and laser arc methods.[21] Raji *et al.* reported carbon dots derived from *Piper betel* leaf as a biomass precursor for the selective detection of Fe^{3+} ions by a fluorometric method.[22] Prakash *et al.* synthesized nitrogen-doped carbon dots using the waste of *Poa pratensis* and performed a selective detection test for dual analytes Mn^{2+} and Fe^{3+} ions with a limit of detection of 1.4 μM and 1.2 μM.[23] Thomas *et al.* fabricated nitrogen-doped carbon dots utilizing *Chionanthus retusus* fruit extract, which showed selectivity for Fe^{3+}, and also investigated its cytotoxicity and bioimaging application.[24] Jiyang *et al.* reported carbon dots derived from the peels of passion fruit and tested these *via* a colorimetric method for the sensitive and selective detection of GSH and L-cysteine, and the synthesized CDs showed peroxidase activity with a limit of detection of 0.62 μM.[25] Jun Li *et al.* synthesized nitrogen and sulfur co-doped carbon dots and designed a switch on–off–on probe for the detection of GSH, and then checked the efficacy of the probe with an actual sample of fetal bovine serum.[26] Further, Wang *et al.* reported gold-decorated carbon dot clusters for the selective detection of glutathione with limit of detection of 2.02 μM.[27] Kaimal *et al.* synthesized graphene based CQDs with amine-functionalized nanoparticles for the sensitive detection of GSH.[28] Recently, Liang *et al.* reported biomass-derived carbon dots using *Wedelia trilobata* for the detection of glutathione and further assessed their imaging application in living cells.[29] All these reports from literature highlight the significance of the detection of GSH. As far as the synthesis protocol is concerned, Sim *et al.* synthesized carbon dots by subjecting a mixture of pineapple juice and ethanol to hydrothermal treatment for 8 h at 120 °C.[30] Similarly, Gupta *et al.* synthesized carbon dots using pineapple juice by the addition of 34 N H_2SO_4 at 100 °C for 60 min to yield blue-emissive carbon dots and 40 N H_3PO_4 at 80 °C for 30 min and 15 min, respectively, to obtain green and yellow emissive carbon dots.[31] However, both of these synthesis methods relied on the use of aggressive chemicals and elevated reaction conditions. In the present study, biomass-derived carbon dots were synthesized from *Ananas Comosus* as a precursor using a microwave synthesizer. The synthesis protocol followed a pure green methodology without the use of any chemicals, which highlights the uniqueness of this work.

A nanoprobe was developed that was environmentally benign, facile, and cost-effective. The as-formed CQDs were stable and displayed excellent selectivity toward different analytes of Mn(VII) ions and GSH. To the best of our knowledge, this green synthetic methodology for the biomass-derived nanosensor is the first reported, where dual analytes could be detected in the nanomolar range by a fluorescent "ON–OFF–ON" assay.

2. Materials and methods

Pure *Ananas Comosus* juice was bought from a local juice bar without any additives in it. The chemicals $Zn(NO_3)_2$, $Ni(NO_3)_2$, $Hg(NO_3)_2$, $Fe(NO_3)_3$, $Fe(NO_3)_2$, $Cu(NO_3)_2$, $Co(NO_3)_2$, $Ce(NO_3)_2$, $Mn(NO_3)_2$, $KMnO_4$, $MnSO_4$, $CrCl_3$, $PbCl_2$, $K_2Cr_2O_7$, KCl, NaCl, $CaCl_2$, $MgCl_2$ and $AlCl_3$, Na_3PO_4, Na_2S, Na_3AsO_4, $Na_2S_2O_5$, $NaNO_2$, $NaNO_3$, $NaHSO_4$, NaCl, HCl, and NaOH were purchased from Loba Chemie Pvt Ltd, India, and were used as received. Amino acids, namely L-aspartic acid, L-arginine, L-leucine, L-glutamine, and L-cysteine, were procured from Spectrochem Pvt

Ltd Mumbai, while glycine, sucrose (AR), glucose (AR), ascorbic acid, glutathione, and dopamine were purchased from Loba Chemie Pvt Ltd, India. All the stock solutions of analytes were prepared in ultrapure deionized water and the amino acids and biomolecules were used without further purification.

2.1. Synthesis of AC-CQDs

Carbon dots were synthesized using a one-step microwave heating using *Ananas Comosus* as the precursor. Fresh juice of *Ananas Comosus* was taken and refrigerated for 3–4 h. Then, the refrigerated juice was sonicated using an ultrasonic cleaner (Labman Scientific instruments) for 20 min. After this, 10–15 mL of the above solution was transferred into a microwave glass reaction vial, which was sealed, and kept in a microwave synthesizer (Biotage microwave synthesizer). The reaction parameters for the temperature and time were set as 150 °C for 1 h. The obtained solution was purified *via* centrifugation (Research Centrifuge, REMI) at 7000 rpm and the supernatant was subjected to filtration using a 0.22 μm syringe filter, and was abbreviated as AC-CQDs (Scheme 1). Next, the solution was kept in 5 days dialysis using a HI-MEDIA Dialysis Membrane-110 LA395-1MT.

2.1.1 Instrumentation. The absorption spectra of the synthesized AC-CQDs were obtained using a UV-Visible spectrophotometer (Shimadzu UV 2450). The PL emission spectra were recorded using a spectrofluorometer (Shimadzu RF-6000). The presence of different surface functional groups of the AC-CQDs was checked using a Fourier transform-infrared spectrophotometer (Shimadzu IRTracer-100). The amorphous structure of the prepared CQDs was examined using X-ray diffraction (XRD, Smart Lab SE) using Cu Kα ($\lambda = 1.540$) as the radiation source ($0 \leq 2\theta \leq 90°$). The size and surface morphology of the CQDs were characterized by transmission electron microscopy (Jeol, JEM 2100 plus). The elemental composition and surface oxidation states were verified *via* X-ray photoelectron spectroscopy (PHI 5000 Versa Probe III). The surface charge (zeta potential) of the synthesized CQDs was evaluated using a Brookhaven 90 Plus particle-size analyzer. Surface defects were investigated using a Raman spectrometer using 532 nm laser radiation. Fluorescence lifetime decay studies were executed on a Delta-Flex modular fluorescence lifetime spectrofluorimeter (HORIBA Scientific) using an excitation source of 300 nm (nanoLED) having an instrument response function (IRF) of ~200 ps. Electrochemical studies were performed using Bio-Logic EC lab software with a standard three-electrode system. The experimental setup included a glassy carbon electrode (GCE), onto which the sample was drop-cast to serve as the working electrode, a standard calomel electrode (SCE) as the reference electrode, and a platinum wire as the counter electrode. All the electrodes were immersed in 1 M KCl electrolyte solution. The cyclic voltammogram (CV) measurements were recorded in the 1 M KCl electrolyte solution using a constant scan rate of 80 mV s^{-1} within the potential range of −0.4 V to +0.4 V.

2.2. Evaluation of the fluorescence quantum yield

The quantum yield (QY) of the AC-CQDs was measured by taking quinine sulfate[32] as a reference ($\phi_R = 0.546$) and was calculated using the equation given below:

$$\phi_S = \phi_R \times \frac{A_S}{A_R} \times \frac{(abs)_R}{(abs)_S} \times \frac{{\eta_S}^2}{{\eta_R}^2} \quad (1)$$

where 'ϕ_S' and 'ϕ_R' signify the fluorescence quantum yields of the AC-CQDs and reference (quinine sulfate), 'Abs' and '*A*' represent the absorbance and area under the fluorescence emission, and the subscripts 'S' and 'R' denote the sample (AC-CQDs) and reference, respectively.

2.3. Determination of the average lifetime value

Average lifetime values for different systems, such as AC-CQDs, [AC-CQDs + Mn(VII)] complex, and [AC-CQDs + Mn(VII) + GSH], were calculated using the equation given below:

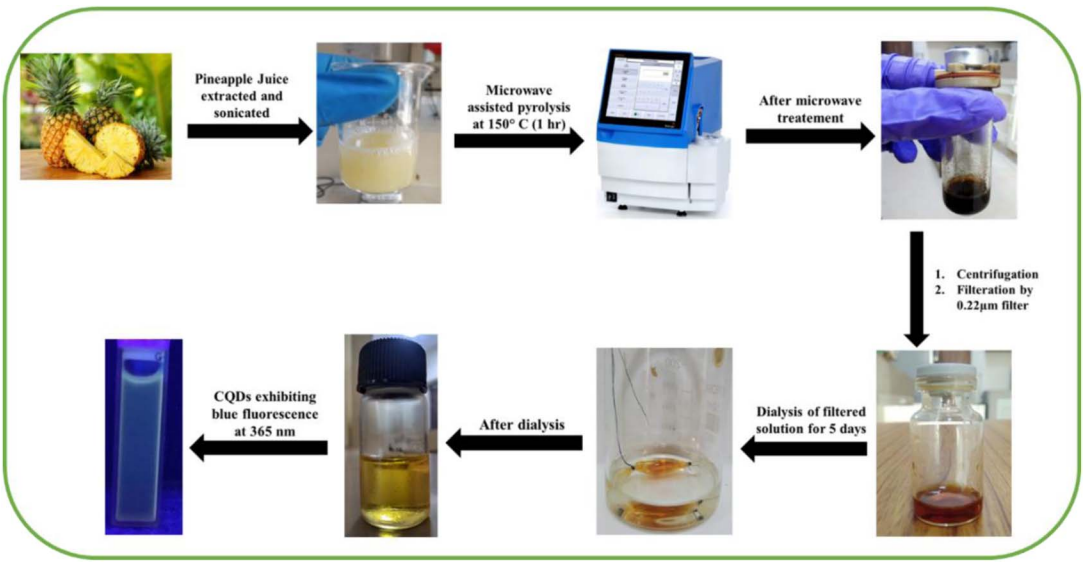

Scheme 1 Green synthetic protocol for obtaining AC-CQDs from pineapple juice (*Ananas Comosus*).

$$\langle\tau\rangle_{avg} = \sum a_i\tau_i \quad (2)$$

where 'a_i' represents the relative population and 'τ_i' signifies the respective lifetime components. To get insights into the quenching mechanism, radiative (k_r) and non-radiative (k_{nr}) rate constants with the quantum yield (ϕ) and average lifetime ($\langle\tau\rangle_{avg}$) were also calculated using the below equations.[33]

$$k_r = \frac{\phi_f}{\langle\tau\rangle_{avg}} \quad (3)$$

$$\frac{1}{\langle\tau\rangle_{avg}} = k_r + k_{nr} \quad (4)$$

2.4. General layout of the experiments

Initially, from the stock of AC-CQDs, 30 μL of CQDs was pipetted out in a cuvette followed by the addition of 2000 μL of distilled water. To this, a fixed amount (100 μL) of different metal ion solutions of fixed concentrations was added respectively to evaluate fluorescence quenching. Similarly, restoration of the fluorescence intensity was investigated by subjecting the quenched solution to various concentrations of glutathione (GSH). All the emission spectra were recorded at an excitation wavelength of 340 nm (λ_{exc} = 340 nm).

3. Results and discussion

3.1. Characterization of the synthesized AC-CQDs

Functional groups on the surface of the synthesized AC-CQDs were identified using their FT-IR spectrum. A broad peak at 3254 cm^{-1} appeared due to the stretching vibration of the –O–H/N–H bands. The sharp peak at 1640 cm^{-1} indicated the presence of either C=O (stretching)/N–H (bending) of the amide group. The peak centered at 1052 cm^{-1} was attributed to C–O (stretching) of the ether group/C–N stretching (Fig. 1a).[34] All these signals affirmed different functional groups were attached to the surface of the AC-CQDs.

Fig. 1b illustrates the XRD pattern of the synthesized AC-CQDs. A broad diffraction peak was obtained at 2θ = 23.4°

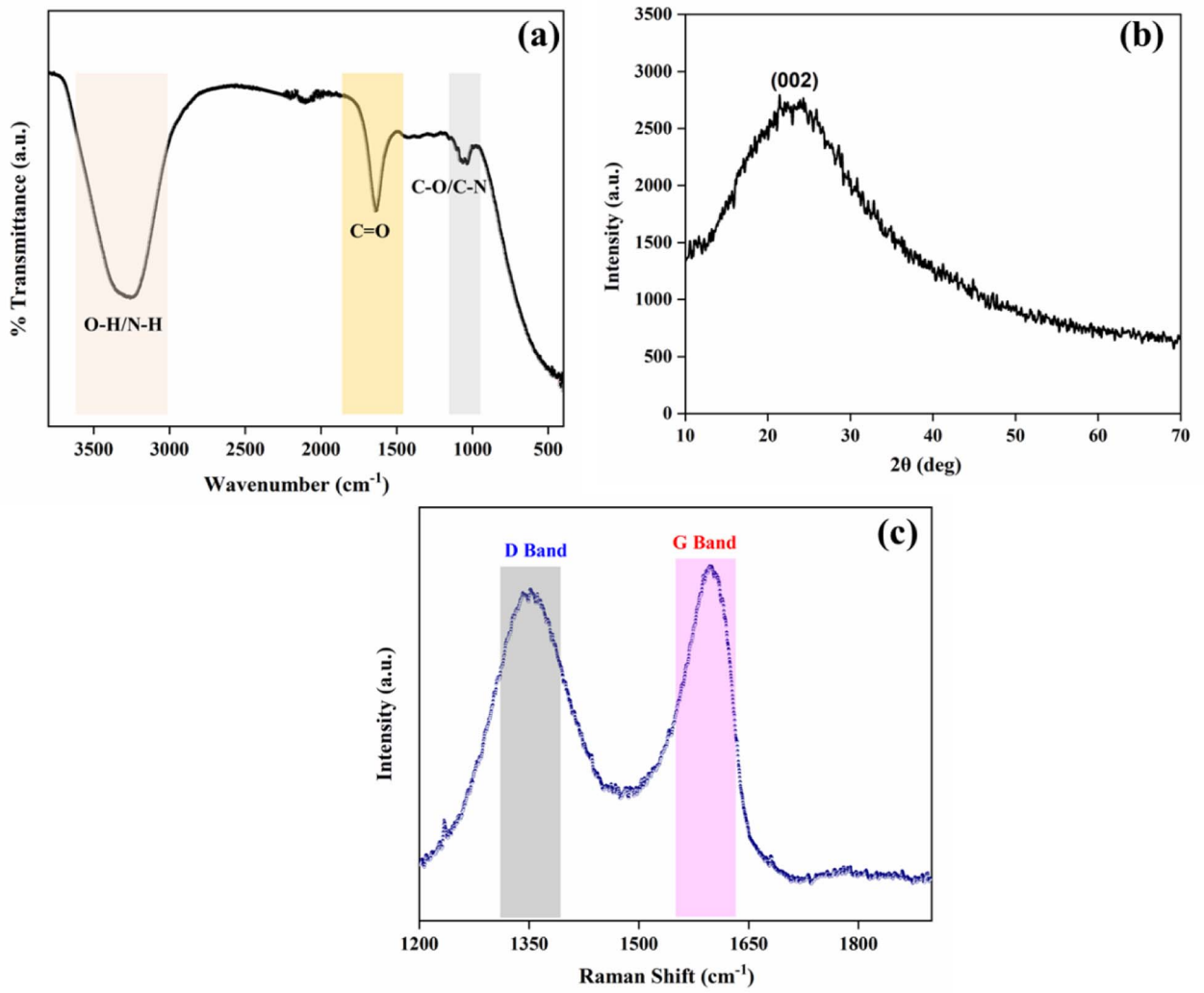

Fig. 1 (a) FTIR spectrum, (b) XRD spectrum, and (c) Raman spectrum of the AC-CQDs.

corresponding to the (002) plane, which is a characteristic peak of graphitic carbon (sp^2 hybridized), indicating the amorphous nature of the CQDs.[35] The absence of any other peak indicated that the synthesized AC-CQDs had good purity and lacked any impurities. The surface defects on the synthesised AC-CQDs were investigated by their Raman spectrum, as shown in Fig. 1c. Two broad peaks with peak positions centred at 1351 and 1597 cm^{-1} were observed, attributed to the defect band (D band) and graphitic band (G band), respectively. The Raman spectral data confirmed the presence of sp^3 (D band) and sp^2 (G band) carbon defects within the AC-CQDs. The disordered-D band was formed by the breathing motion of κ-point phonons with the A_{1g} symmetry, which was caused by defects in the sp^3 carbons, whereas the graphite-G band was produced by the first-order scattering of E_{2g} phonons from sp^2 hybridized carbon atoms.[36] The intensity ratio $I_D : I_G$ was calculated by taking the peak intensities and turned out to be 0.91, indicating the degree of graphitization, which was in accordance with the XRD results.[37,38]

The elemental composition of the synthesized AC-CQDs and their surface oxidation states were analyzed by XPS. The peaks observed at 284.5, 398.9, and 528.9 eV corresponded to C 1s (62.5%), N 1s (2.33%), and O 1s (35.17%), respectively, in the high-resolution survey spectrum (Fig. 2a). Further, upon deconvolution, the C 1s spectrum showed three major peaks, corresponding to C–OH, C=C/C–C, and C–O/C–N/O–C=O (Fig. 2b) at 283.4, 284.8, and 286.2 eV, respectively.[39,40] Similarly, the O 1s spectrum (Fig. 2c) exhibited peaks at 530.8 and 531.9 eV and the peaks were assigned to C–O and C=O.[41,42] The peaks at 398.8 and 400.5 eV in the N 1s spectrum (Fig. 2d) were attributed to C–N–C and N–H.[29] The intrinsic nitrogen functionalization of the AC-CQDs was accredited to the presence of carotenoids, flavonoids, alkaloids, folates, vitamin B_1, vitamin B_6, *etc.*, present in *Ananas Comosus* and acted as a source of nitrogen.[43]

The size and the surface morphology of the AC-CQDs was obtained using HR-TEM analysis. Fig. 3a and c illustrate the formation of carbon dots with particle sizes ranging from 1 to 4.5 nm.[44] Fig. 3b shows the histogram depicting the particle-size distribution, with an average particle size of 2.25 ± 0.97 nm. Furthermore, the zeta potential value (Fig. S1a†) was found to be −6.17 mV, which confirmed that the synthesized AC-CQDs contained negatively charged functional groups on the surface.[45]

3.2. Optical properties of the AC-CQDs

The photophysical properties of the synthesised AC-CQDs were studied by recording their UV-visible absorption spectrum, as

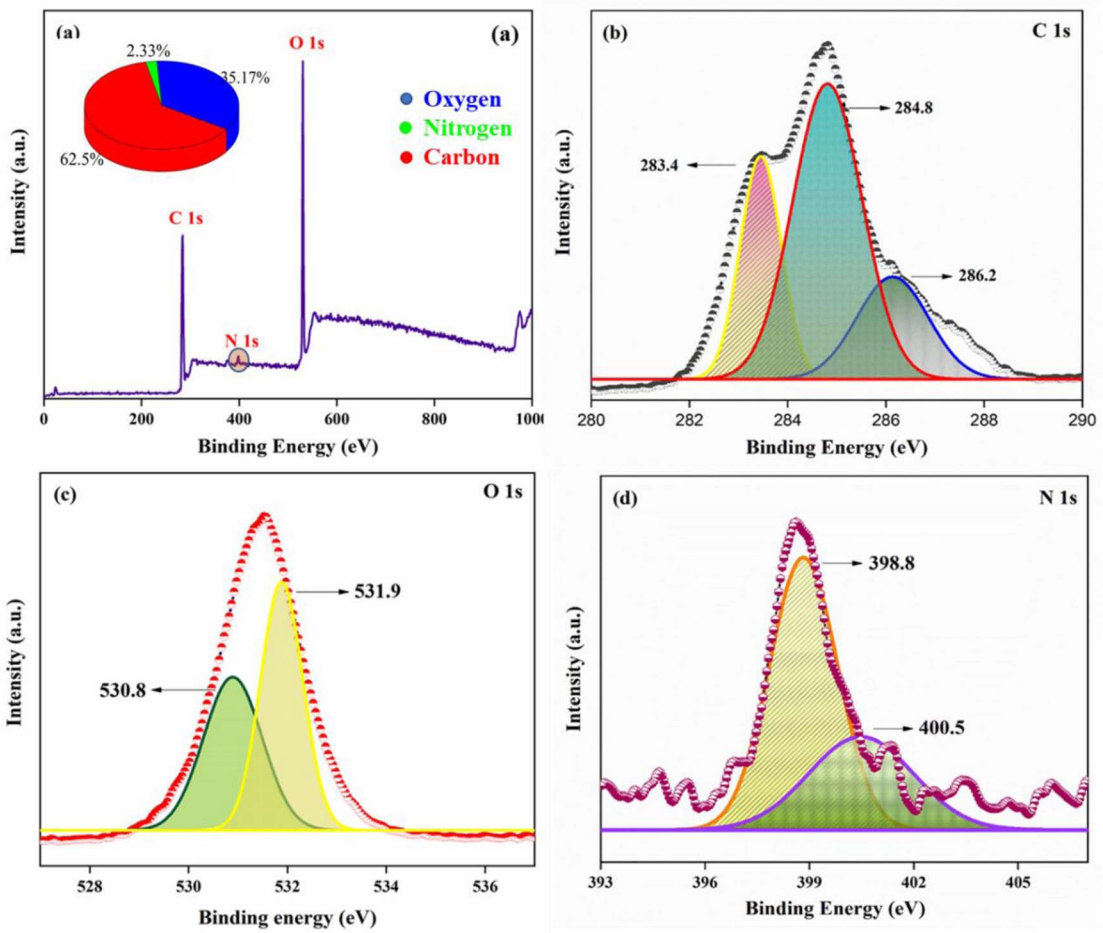

Fig. 2 (a) High-resolution survey spectrum of XPS, (b) C 1s spectrum, (c) O 1s spectrum, and (d) N 1s spectrum of the AC-CQDs.

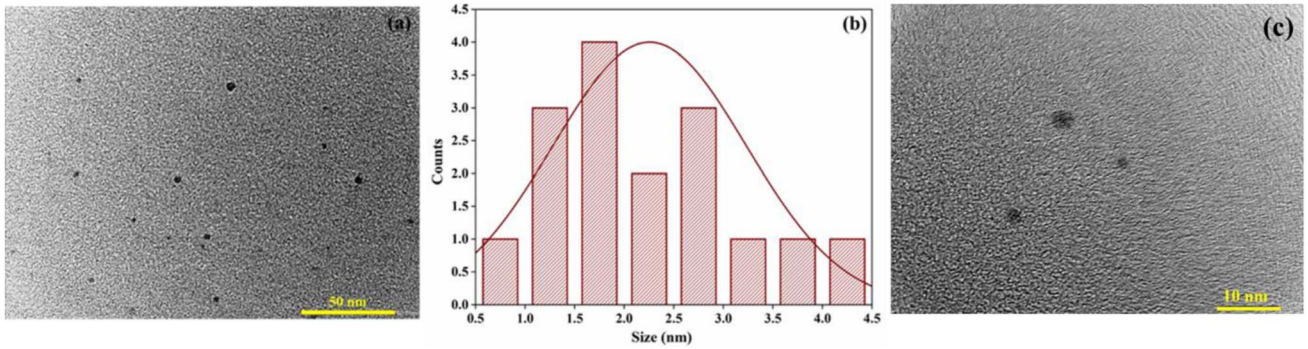

Fig. 3 HR-TEM image (a) at 50 nm and (b) histogram depicting the particle size, and (c) HR-TEM image at 10 nm resolution.

well as their fluoroscence spectrum. Fig. 4a shows a weak absorption peak appeared at 265 nm, which was attributed to π–π* transition of the sp^2 hybridized carbon core, while the predominant peak at 324 nm signified n–π* transition of C=O.[46,47] In aqueous medium, the AC-CQDs displayed a yellow colour in the visible region, but when exposed to UV radiation at 365 nm, blue-emissive fluorescence was observed (Fig. 4a inset). The fluorescence emission of the AC-CQDs can be explained on the basis of the photoinduced charge separation and trapping at the surface sites, which caused a radiative recombination mechanism between holes and electrons.[48,49]

Fig. 4b shows the maximum fluorescence intensity with excitation (λ_{ex}) and emission maxima (λ_{em}) appeared at 340 nm and 422 nm, respectively (Fig. 4b). The fluorescence quantum yield of the synthesized AC-CQDs (using eqn (1)) showed a significantly high PLQY value of ~48% (Table 1). Fig. 4c shows the excitation-dependent emission properties of the AC-CQDs. Upon gradually increasing the excitation wavelength from 280

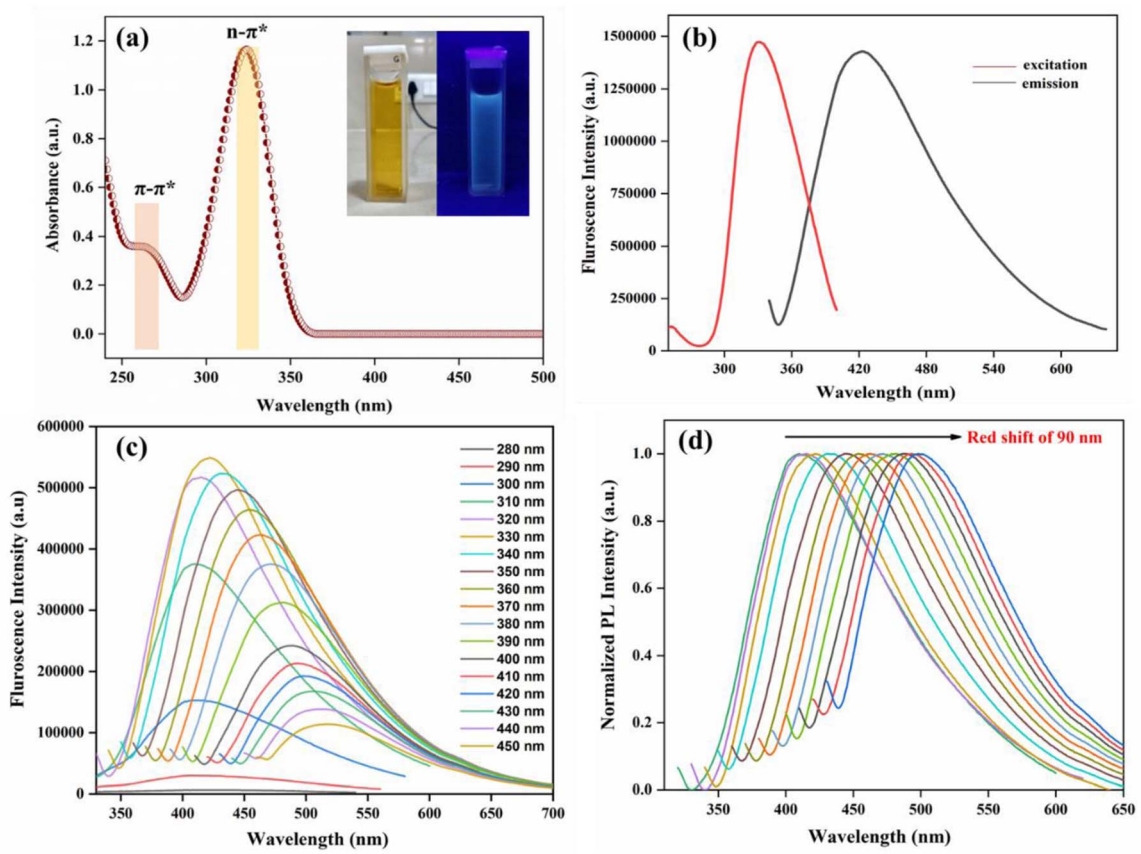

Fig. 4 (a) UV-vis absorption spectrum of the AC-CQDs, with the inset showing the solution under visible (left) and UV light (right) illumination; (b) excitation and emission spectra; (c) excitation wavelength-dependent emission spectra; and (d) normalised emission spectral shifts of the AC-CQDs.

Table 1 Photophysical parameters of the AC-CQDs in the presence of different systems

Systems	Quantum yield (%)	$\langle\tau_{avg}\rangle$	k_r (ns^{-1})	k_{nr} (ns^{-1})	K_{S-V}[a] (nM^{-1})	K^b (nM^{-1})
AC-CQDs	48	4.93	0.097	0.105	—	—
AC-CQDs @ Mn(VII)	21	3.64	0.057	0.217	0.00743	5911
[AC-CQDs @ Mn(VII)] + GSH	37	4.53	0.081	0.139	—	1241

[a] Stern–Volmer constant. [b] Binding constant, error limit = ±5%.

to 450 nm, the emission wavelength underwent a bathochromic shift. Fig. 4d displays the huge bathochromic shift of the emission wavelength from 409 nm to 499 nm. This excitation-dependency emission characteristic property of the synthesized AC-CQDs could be attributed to the surface defects, aromatic structures,[50] zig-zag sites, quantum confinement phenomenon,[51] and non-uniform size distribution.

3.3. Evaluation of the stability of the AC-CQDs

For an ideal fluorescence-based nanosensor, the stability is one of the most important parameters to be considered prior to application. The photostability of the AC-CQDs was thus checked by fluorescence studies. Fig. S1b† shows the effect of pH variation on the fluorescence emission intensity. It was observed that the inherent pH of the AC-CQDs was 4, and upon changing the pH range from 4 to 7, a gradual rise in PL intensity was noticed. The maximum intensity was obtained at neutral pH 7, followed by a decline in intensity in basic pH from 8 to 12. This change in PL intensity occurred due to protonation and deprotonation of the sites of the AC-CQDs responsible for causing the emission.[52,53] The maximum fluorescence intensity observed at neutral pH medium may be rationalized due to the formation of zwitterionic species between hydroxyl/carboxylic acid/amine functional groups (as analyzed by FTIR and XPS) on the surface of the AC-CQDs. Therefore, the proposed nanosensor may be applied in physiological medium. Furthermore, after being irradiated for approximately 90 min, no change in the PL intensity was observed for the AC-CQDs, as shown in Fig. S1c,† indicating a good photobleaching property.[54] Moreover, the effect of ionic strength with different concentrations of NaCl was examined. The emission peak position and PL intensity remained unaltered (Fig. S1d†). Besides this, the stability of AC-CQDs was observed for a period of 5 months and the peak positions remained intact, indicating a high stability (Fig. S2†). All these studies confirmed that the synthesized AC-CQDs were stable and suitable for further sensing applications.

3.4. Selectivity studies

Selectivity is a crucial parameter for the development of a novel nanosensor. To comprehend the effect of selectivity, 1 mM stock of different metal ions (Zn(II), Ni(II), Hg(II), Fe(III), Fe(II), Cu(II), Co(II), Ce(III), Mn(II), Mn(VII), Cr(III), Pb(II), Cr(VI), K(I), Ca(II), Na(I), Mg(II), and Al(III)) was prepared. After that, 30 μL of AC-CQDs was transferred in a cuvette, followed by the addition of 100 μL of the respective metal ion solutions and the volume was adjusted to 2 mL with distilled water. Next, the variation of the fluorescence intensity of the AC-CQDs was recorded at λ_{exc} = 340 nm. As depicted in Fig. 5a, the results showed that out of all the metal ions, Mn(VII) quenched the PL intensity most. Consequently, further titrations of Mn(VII) ions were performed, as the rest of the metal ions showed a minimal response. The PL response of the AC-CQDs in the presence of various anions (Cl^-, I^-, AsO_4^{3-}, NO_2^-, NO_3^-, HSO_4^-, $S_2O_5^{2-}$, S^{2-}, PO_4^{3-}) was also studied to demonstrate their selectivity towards anions (Fig. 5b). The outcomes of the experiment revealed that changing different anions had no effect on the PL intensity of the AC-CQDs. Thus, the study clearly confirmed that the synthesized AC-CQDs were highly selective and a potent nanosensor for Mn(VII) ions. Furthermore, to account for the greater selectivity, an interference study for the AC-CQDs for Mn(VII) was performed (Fig. S5a†) in the presence of different metal ions in the ratio of 1 : 3, which revealed that none of the metal ions significantly interfered with Mn(VII) detection.

3.5. Elucidation of the selectivity of the AC-CQDs with Mn(VII) ions

Fig. 5c clearly demonstrated that the fluorescence intensity was substantially quenched (~6.5 folds) with the gradual incorporation of Mn(VII) ions in the nanomolar range. From Table 1, it was found that the highly fluorescent AC-CQDs (ϕ_f = 48%) turned into a less fluorescent complex in the presence of Mn(VII) ions (ϕ_f = 21%). In addition, the radiative rate constant (k_r) of the AC-CQDs was significantly quenched while the non-radiative rate constant (k_{nr}) was substantially enhanced in the presence of Mn(VII) ions, clearly confirming the fluorescence turn-off phenomenon. The preferential quenching of AC-CQDs towards Mn(VII) ions was due to multisite interactions between the Mn(VII) ions and the electron-rich functional moieties of the carbon dots. Mn(VII) ions were coordinated *via* chelation with O and N functional groups on the surface of the AC-CQDs, as well as the π-system of the sp^2 domains of the CQDs.[55,56] In addition, AC-CQDs included more oxygen-containing (35.17% oxygen from the XPS analysis) functional groups, which could act as excellent electron donor sites and transfer electrons to the vacant 3d-orbital of the highly electron-deficient species, *i.e.* Mn(VII) ions, resulting in electron–hole (e^-–h^+) pair recombation,[57] which eventually quenched the PL intensity by forming a weak-fluorescent [AC-CQDs@Mn(VII)] complex (Scheme 2). To gain deeper insights into the interaction mechanism, TCSPC measurements were performed. The average lifetime value of the AC-CQDs was significantly quenched from 4.93 ns to 3.64 ns in the presence of Mn(VII) ions (Table 1). This results clearly

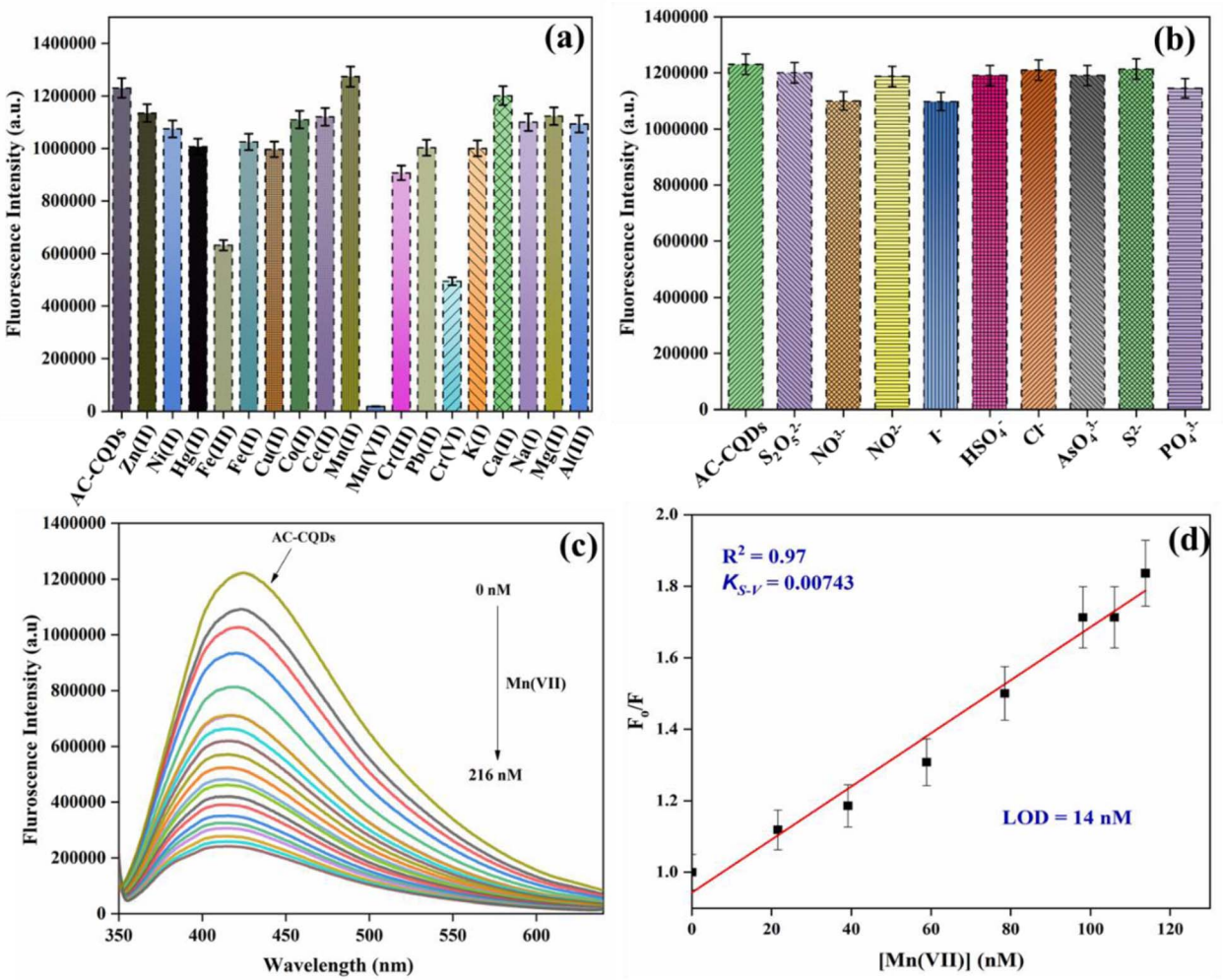

Fig. 5 Selectivity of the synthesized AC-CQDs with (a) different cations, (b) different anions, (c) variation in the fluorescence intensity of the AC-CQDs with different concentrations of Mn(VII) ions, and (d) plot of F_0/F against [Mn(VII)] ions for determination of the LOD value for Mn(VII) ions.

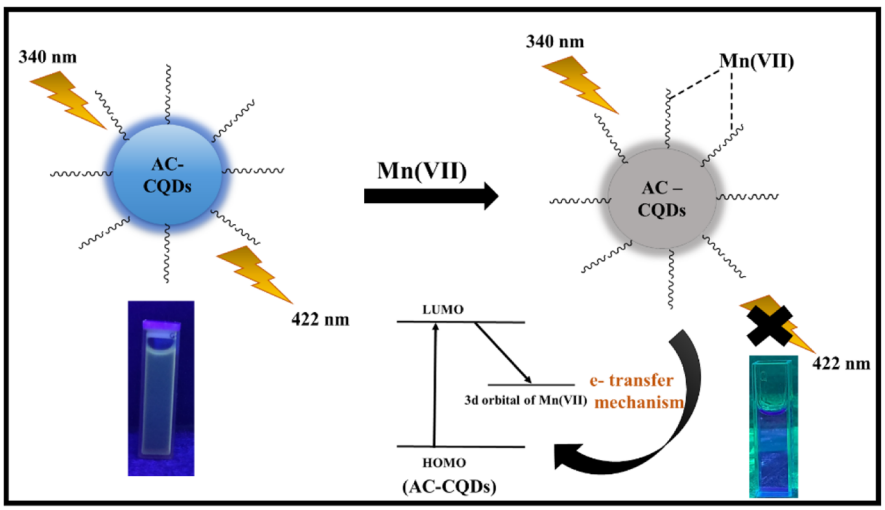

Scheme 2 Illustration of the sensing of Mn(VII) ions by AC-CQDs *via* a turn-off mechanism.

confirmed that the AC-CQDs showed a dynamic quenching mechanism with Mn(VII) ions.[33,58] Moreover, the effect of temperature on the AC-CQDs was analyzed over a range of 20 °C to 80 °C (Fig. S6†). With every 10 °C increment in temperature, a substantial dip in fluorescent intensity was observed, as higher temperature accelerated the excited state electron-transfer process, which was in direct agreement with dynamic quenching.[59]

3.6. Determination of the sensitivity and photophysical parameters of the [AC-CQD@Mn(VII)] nanosensor

In practical applications, a reliable nanosensor requires not only high selectivity, but also high sensitivity to the analyte. From the linear plot of F_0/F against [Mn(VII)] ions, the limit of detection (LOD) value for Mn(VII) ions was calculated (Fig. 5d) by using the value of $3\sigma/K$, where 'σ' represents the standard deviation of the intercept and 'K' denotes the slope. The LOD value was found to be 14 nM with a linearity range of 0–120 nM. Table 2 demonstrates that the prepared sensor had a high sensitivity to Mn(VII) ions and a low detection limit compared to other sensor systems described in the literature.[60–63]

Further, to comprehend the quenching efficiency of the [AC-CQDs@Mn(VII)] nanosensor, the Stern–Volmer quenching constant (K_{S-V}) was estimated using the following equation:

$$\frac{F_0}{F} = 1 + K_{S-V}[Q] \quad (5)$$

The graph between $\frac{F_0}{F}$ and [Q] displayed a linear plot, in which the slope value presented the quenching constant (K_{S-V}). The terms 'F_0' and 'F' denote the fluorescence intensity in the absence and presence of the quencher, while 'Q' refers to the concentration of the quencher, *i.e.* Mn(VII) ions, and 'K_{S-V}' is the Stern–Volmer constant. The 'K_{S-V}' value was estimated to be 0.00743 nM^{-1}, with a correlation coefficient (R^2) of 0.97, signifying that the nanosensor had an acceptable linearity range (Fig. 5d). The linear regression equation for the Stern–Volmer equation was:

$$\frac{F_0}{F} = 0.00743[Mn^{7+}] + 0.94298 \quad (6)$$

In order to understand the interaction between the AC-CQDs and Mn(VII) ions, the Benesi–Hildebrand 1 : 1 stoichiometry model with the following equation[64] was used:

$$\frac{1}{F_0 - F} = \frac{1}{F_0 - F_1} + \frac{1}{K[Q](F_0 - F)} \quad (7)$$

where F_0 and F signify the fluorescence intensity of the AC-CQDs and AC-CQDs with the gradual addition of Mn(VII) ions, F_1 represents the intensity of the 1 : 1 complex formed by [AC-CQDs + Mn(VII)], Q denotes the concentration of Mn(VII) ions, and K_1 is the binding constant value of the [AC-CQDs@Mn(VII)] complex. The binding constant value (K_1) was derived from the plot of ($1/F_0 - F$) against ($1/Q$) by taking the reciprocal of the slope of the graph, and the calculated value is tabulated in Table 1 and shown in Fig. S3.† The residual fits of the time-resolved fluorescence emission spectra are displayed in Fig. S4,† which show that the lifetime data were well fitted.

3.7. Restoration of the fluorescence for the selective and sensitive detection of GSH

In general, three categories of fluorescence sensing strategies have been developed to determine the sensitivity of nanomaterials to various analytes. One is the direct interaction of CQDs with analytes, which results in a modification in the fluorescence response. The second is the surface functionalization of CQDs with analytes using chemical conjugation approaches to detect analytes. The third is the application of CQDs in conjunction with other sensing analytes. These analytes function as quenchers and combined with the target analyte result in the recovery of fluorescence.[65] In this investigation, the combination of two phenomena, fluorescence quenching and recovery, was used to develop a sensing platform for the precise quantification of dual analytes. This method also facilitates the detection of multiple analytes. In this context, the fluorescence turn-off–on method was employed. To restore the fluorescence intensity of the [AC-CQDs + Mn(VII)] nanoprobe, several amino acids and biomolecules were checked for their fluorescence response. For this, 1 mM stock of several amino acids, namely glutamine (Glt), aspartic acid (Asp), arginine (Arg), glucose (Glu), ascorbic acid (AA), leucine (Leu), sucrose (Suc), cysteine (Cys), glycine (Gly), glutathione (GSH), and dopamine (DA), was prepared. A fixed concentration of each of the analytes was added to the [AC-CQDs@ Mn(VII)] system, and the PL spectra were recorded. The study confirmed that the designed sensing platform [AC-CQDs@ Mn(VII)] was extremely selective and sensitive for GSH detection. As depicted by the selectivity studies in Fig. 5a, a substantial quenching of the PL intensity of the AC-CQDs was seen with Fe(III) and Cr(VI) ions,

Table 2 Comparison of different sensing probes used for the detection for Mn(VII) ions

S. no.	System	Linear range	Detection limit (LOD)	Ref.
1	N,P-doped CDs	10–100 μM	48.3 nM	60
2	N,S,P co-doped CNDs	0.05–20 μM	50 nM	61
3	N,Al-doped CDs	0–100 μM	46.8 nM	62
4	N-doped CDs	5–35 μM	0.66 μM	63
5	AC-CQDs@Mn(VII)	0–120 nM	14 nM	Present work

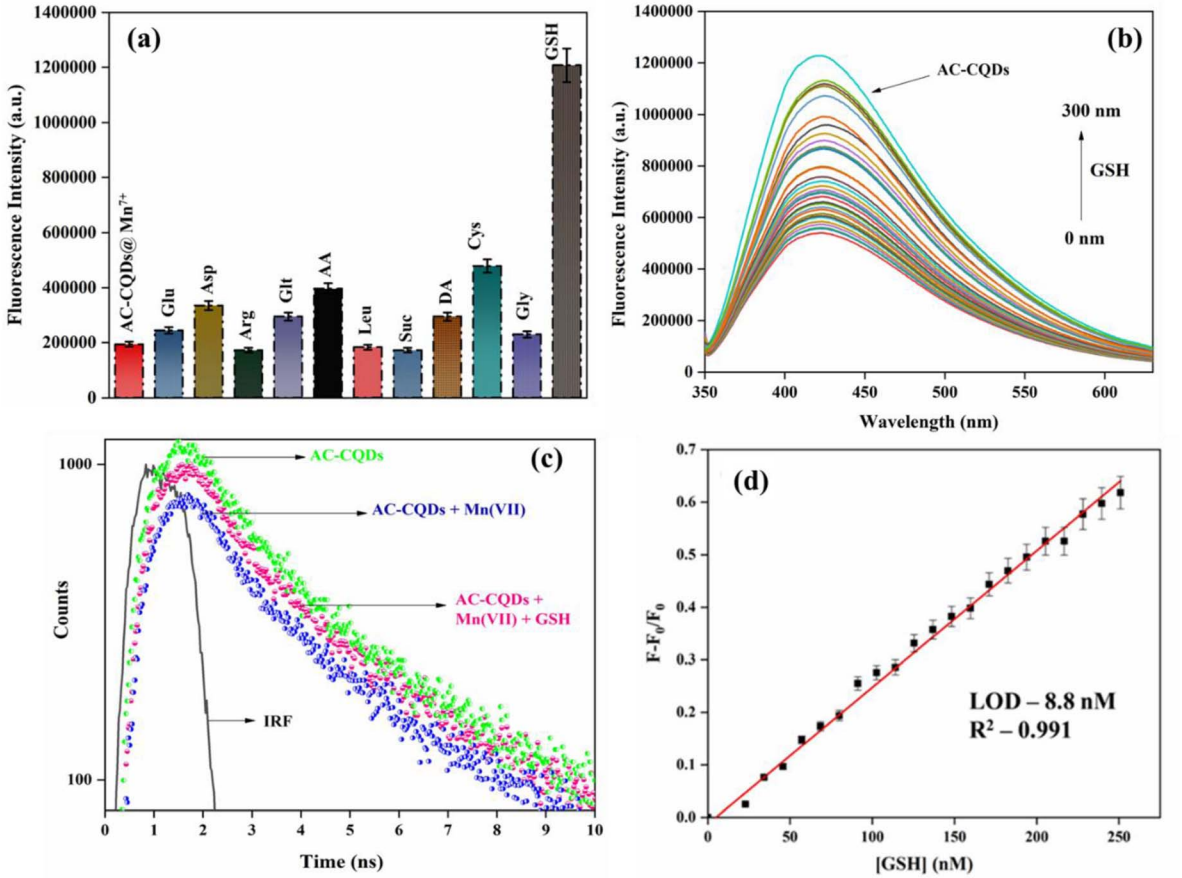

Fig. 6 (a) Turn-on selectivity study with different amino acids and biomolecules, (b) restoration of the PL intensity of the AC-CQDs with the gradual addition of [GSH], (c) lifetime plot, and (d) LOD value for GSH.

and so the fluorescence recovery response of the [AC-CQDs@Fe(III)/Cr(VI)] system towards GSH was also checked (Fig. S7†); whereby a negligible turn-on response was observed compared to with Mn(VII) ions. Fig. 6a displays the turn-on selectivity of GSH, which restored the PL intensity to an appreciable extent. Additionally, to ensure the greater selectivity of the [AC-CQDs@Mn(VII)] system towards GSH, an interference study was performed (Fig. S5b†) through the addition of several amino acids and biomolecules in a 1 : 3 ratio, and it was observed that the designed system showed appreciable selectivity towards GSH. Further, it was observed that upon the gradual addition of GSH in the nanomolar range of up to 300 nM, the PL intensity of the [AC-CQDs@Mn(VII)] nanosensor was enhanced 2.2-fold (Fig. 6b). Upon closer scrutiny, it was found that the PLQY value of the [AC-CQDs@Mn(VII)] nanosensor was increased from 21% to 37% in the presence of GSH (Table 1). The average lifetime value of the nanosensor was dramatically enhanced in the presence of GSH (Fig. 6c and Table 1). The lifetime components and their relative populations in the AC-CQDs in different systems are tabulated in Table S1.† Moreover, the radiative rate constant (k_r) value was significantly enhanced while the non-radiative rate constant (k_{nr}) value was dramatically decreased, which showed the fluorescence intensity of the AC-CQDs was restored in the presence of GSH (Table 1). Besides, paper strip testing was performed by using Whatman filter paper to check the turn-off–on response of the designed system of AC-CQDs under UV illumination (Fig. S8†), which revealed a loss of fluorescence intensity of the AC-CQDs in the presence of Mn(VII) and a recovery of the PL intensity upon the addition of GSH. This also highlighted its potential for security ink purpose. Further, the binding constant value of the [AC-CQDs@Mn(VII)] nanosensor was estimated as 5911 nM^{-1} (Fig. S3a† and Table 1). The binding constant value of the nanosensor in the presence of GSH was significantly lower and found to be 1241 nM^{-1} (Fig. S3b† and Table 1). This result suggests that Mn(VII) ions are driven out from the surface of the AC-CQDs and form a complex with GSH, resulting in fluorescence restoration (Scheme 4). A control experiment was also carried out to test this, which demonstrated that the AC-CQDs were not directly related to the selectivity in GSH detection, as there were only very minor

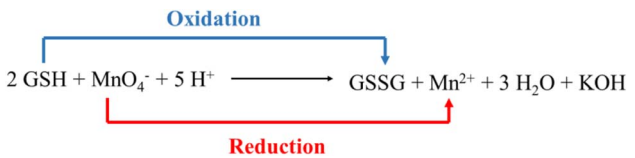

Scheme 3 Redox reaction between Mn(VII) ions and GSH, responsible for fluorescence enhancement.

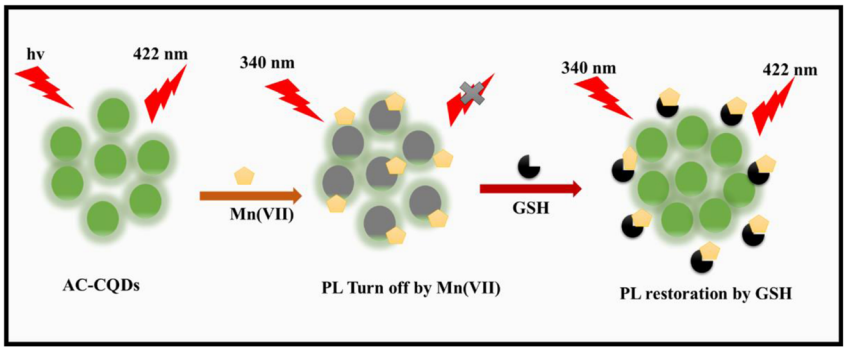

Scheme 4 Mechanism depicting the interaction between [AC-CQDs @Mn(VII)] and GSH.

Table 3 Comparison of different probes used for the detection of GSH

S. No.	System	Linear range	Detection limit (LOD)	Ref.
1	Cellulose CQDs	20–400 μM	5.98 μM	70
2	Au-decorated carbon dot cluster	0–300 μM	2.2 μM	71
3	N-doped graphene CQDs	0.5–0.48 μM	87 nM	72
4	N, S-dual doped CQD	3.8–415.1 μM	0.21 μM	73
5	*Wedelia trilobata* derived CQDs	0–3 mM	35 μM	29
6	AC-CQDs	0–250 nM	8.8 nM	Present work

changes in fluorescence intensity (Fig. S3c†). Additionally, the UV–vis absorption spectra of the AC-CQDs, [AC-CQDs@Mn(VII)], and [AC-CQDs@ Mn(VII)] + GSH were recorded, and revealed that no new substances were formed in the presence of Mn(VII) and GSH, as there was no change in the peak positions (Fig. S9†).[66] A plausible reason for the fluorescence enhancement is a redox reaction taking place between Mn(VII) ions and GSH, leading to the formation of Mn^{2+} and GSSH (glutathione disulfide) as the reduced and oxidized products, as shown in Scheme 3.[67] This observation was supported by further electrochemical studies; whereby the bare AC-CQDs showed a large CV area, indicating good stability,[68] but upon the addition of GSH to AC-CQDs@Mn^{7+}, a distinct redox peak was observed, attributed to the surface structure of the AC-CQDs, which indicated electron transfer of the redox couple, as shown in Fig. S10.†[69] The findings clearly confirmed that the [AC-CQDs@Mn(VII)] nanosensor was highly selective for the detection of GSH in the nanomolar range. Further, the limit of detection (LOD) value was calculated for the sensitive detection of GSH. A good linear range was found (0–250 nM) from the plot between $(F - F_0/F_0)$ against [GSH]. The estimated LOD value was found to be 8.8 nM (Fig. 6d), with a high correlation coefficient ($R^2 = 0.991$). The prepared nanosensor exhibited a high sensitivity towards GSH and significantly lower detection limit compared to other nanosensors reported in the literature, as shown in Table 3.

3.8. Determination of the precision and accuracy

Interday and intraday precision analysis was executed to determine the error and relative standard deviation (%RSD). Triplicates of different concentrations were considered for both Mn(VII) and GSH. Errors less than 2% indicated the precision of the developed sensor (Table S2†).

3.9. Real sample analysis

To check the viability of the developed probe, the detection of Mn(VII) in real samples was performed. For this, river water was taken from the Bakhra river, Patiala, and tap water. Both these samples were spiked with a known concentration of Mn(VII) (Table S3†). The data indicated acceptable recovery percentage and relative standard deviation (%RSD) values, confirming its potential for the selective detection of Mn(VII) ions in real samples.

4. Conclusion

In the present study, an eco-friendly, green, and cost-effective methodology was employed to synthesize highly fluorescent intrinsic nitrogen-functionalized CQDs (PLQY 48%) from biomass waste (pineapple juice) using microwave irradiation without the use of any chemicals. The synthetic protocol involved a straightforward method and produced a stable product that exhibited blue emission under UV light and wavelength-dependent emission properties. The average diameter of the AC-CQDs was found to be 2.25 nm from TEM analysis. Moreover, the synthesized AC-CQDs were characterized by XRD, XPS, Raman, and FTIR spectroscopic techniques. The synthesized AC-CQDs were highly selective and sensitive for Mn(VII) ions, with an 85% quenching efficiency in the nanomolar range. The quenching was confirmed to

occur by a dynamic quenching mechanism from the TCSPC results. The detection limit of Mn(VII) ions was found to be 14 nM, with a linearity range of 0–120 nM. In addition, the developed [AC-CQDs@ Mn(VII)] nanosensor showed a sensitive detection performance for GSH in the nanomolar range by a fluorescence restoration approach. The LOD value was estimated to be 8.8 nM, with a linear concentration range of 0–250 nM. In summary, biomass-derived CQDs were developed for the detection of dual analytes by a fluorescence turn-off–on mechanism and could be employed in the nanomolar range. Besides, the feasibility of the designed nanosensor was examined by carrying out paper strip testing as well as validation with real water samples. The current findings should pave the way for a sustainable and rapid approach to be used as an effective strategy with significant economic and environmental benefits and with standard precision and accuracy.

Conflicts of interest

The authors declare that they do not have any conflicts of interest in the publication of the manuscript.

Acknowledgements

M. P. is thankful to Thapar Institute of Engineering and Technology, Patiala for the fellowship and infrastructural facilities. B. M. acknowledges financial assistance from the Science and Engineering Research Board (SERB) for SRG grant (SRG/2022/000942) as well as TIET, Patiala for seed money. We are also grateful to TIET-VT CEEMS for FTIR analysis, CIL, Panjab University, Chandigarh for HR-TEM analysis, IIT Roorkee for XPS facility, SPMS, TIET for XRD and Raman analysis. The authors acknowledge Prof. Vijay Laxmi for allowing TCSPC facility and Prof. Bhupendra Kumar Chudasama for zeta potential measurement. We gratefully acknowledge the assistance provided by Prof. O. P. Pandey for conducting the electrochemical analysis.

References

1 N. Sohal, B. Maity and S. Basu, *ACS Appl. Nano Mater.*, 2020, **3**, 5955–5964, DOI: **10.1021/acsanm.0c01088**.
2 X. Yan, Y. Song, C. Zhu, J. Song, D. Du, X. Su and Y. Lin, *ACS Appl. Mater. Interfaces*, 2016, **8**, 21990–21996, DOI: **10.1021/acsami.6b05465**.
3 Y. Wang, L. Jiang, Q. Leng, Y. Wu, X. He and K. Wang, *Biosens. Bioelectron.*, 2016, **77**, 914–920, DOI: **10.1016/j.bios.2015.10.071**.
4 L. He, Q. Xu, Y. Liu, H. Wei, Y. Tang and W. Lin, *ACS Appl. Mater. Interfaces*, 2015, **7**, 12809–12813, DOI: **10.1021/acsami.5b01934**.
5 C. B. Pocernich and D. A. Butterfield, *Biochim. Biophys. Acta*, 2012, **1822**, 625–630, DOI: **10.1016/j.bbadis.2011.10.003**.
6 P. S. Samiec, C. D. Botsch, E. W. Flagg, J. C. Kurtz, P. Sternberg, R. L. Reed and D. P. Jones, *Free Radical Biol. Med.*, 1998, **24**(5), 699–704, DOI: **10.1016/S0891-5849(97)00286-4**.
7 Q. Y. Cai, J. Li, L. Zhang, Y. L. Hu, Z. H. Li and L. B. Qu, *Biosens. Bioelectron.*, 2015, **72**, 31–36, DOI: **10.1016/j.bios.2015.04.077**.
8 P. Kubalczyk and E. Bald, *Electrophoresis*, 2009, **30**, 2280–2283, DOI: **10.1002/elps.200800741**.
9 G. G. Huang, X. X. Han, M. K. Hossain and Y. Ozaki, *Anal. Chem.*, 2009, **81**, 5881–5888, DOI: **10.1021/ac900392s**.
10 R. Jia, K. Jin, J. Zhang, X. Zhen, S. Wang and J. Zhang, *Sens. Actuators, B*, 2020, **321**, 128506, DOI: **10.1016/j.snb.2020.128506**.
11 N. K. Wawegama, G. F. Browning, A. Kanci, M. S. Marenda and P. F. Markham, *Clin. Vaccine Immunol.*, 2013, **21**, 196–202, DOI: **10.1128/CVI.00670-13**.
12 Y. Xu, X. Niu, H. Zhang, L. Xu, S. Zhao, H. Chen and X. Chen, *J. Agric. Food Chem.*, 2015, **63**, 1747–1755, DOI: **10.1021/jf505759z**.
13 N. Shao, J. Jin, H. Wang, J. Zheng, R. Yang and W. Chan, *J. Am. Chem. Soc.*, 2010, **132**, 725–736, DOI: **10.1021/ja908215t**.
14 Y. Wang and A. Hu, *J. Mater. Chem. C*, 2014, **2**, 6921–6939, DOI: **10.1039/c4tc00988f**.
15 Y. Wang, Z. Li, D. Hu, C. Lin, J. Li and Y. Lin, *J. Am. Chem. Soc.*, 2010, **132**, 9274–9276, DOI: **10.1021/ja103169v**.
16 X. Yan, H. Li, X. Han and X. Su, *Biosens. Bioelectron.*, 2015, **74**, 277–283, DOI: **10.1016/j.bios.2015.06.020**.
17 J. Zhu, X. Song, L. Gao, Z. Li, Z. Liu, S. Ding, S. Zou and Y. He, *Biosens. Bioelectron.*, 2014, **53**, 71–75, DOI: **10.1016/j.bios.2013.09.036**.
18 X. L. Zhang, C. Zheng, S. S. Guo, J. Li, H. H. Yang and G. Chen, *Anal. Chem.*, 2014, **86**, 3426–3434, DOI: **10.1021/ac500336f**.
19 R. Deng, X. Xie, M. Vendrell, Y. T. Chang and X. Liu, *J. Am. Chem. Soc.*, 2011, **133**, 20168–20171, DOI: **10.1021/ja2100774**.
20 M. Zulfajri, H. N. Abdelhamid, S. Sudewi, S. Dayalan, A. Rasool, A. Habib and G. G. Huang, *Biosensors*, 2020, **10**(6), 68, DOI: **10.3390/bios10060068**.
21 N. Sohal, B. Maity and S. Basu, *ACS Appl. Bio Mater.*, 2021, **4**, 5158–5168, DOI: **10.1021/acsabm.1c00353**.
22 R. Atchudan, T. N. J. I. Edison, S. Perumal, R. Vinodh and Y. R. Lee, *J. Mol. Liq.*, 2019, **296**, 111817, DOI: **10.1016/j.molliq.2019.111817**.
23 P. Krishnaiah, R. Atchudan, S. Perumal, E. S. Salama, Y. R. Lee and B. H. Jeon, *Chemosphere*, 2022, **286**, 131764, DOI: **10.1016/j.chemosphere.2021.131764**.
24 R. Atchudan, T. N. J. I. Edison, D. Chakradhar, S. Perumal, J. J. Shim and Y. R. Lee, *Sens. Actuators, B*, 2017, **246**, 497–509, DOI: **10.1016/j.snb.2017.02.119**.
25 L. Junxue, W. Yufei, M. A. Wenyan, Z. Siyu and L. Jiyang, *Chem. Res. Chin. Univ.*, 2022, **38**(6), 1446–1452, DOI: **10.1007/s40242-022-2021-1**.
26 H. Qi, X. Sun, T. Jing, J. Li and J. Li, *RSC Adv.*, 2022, **12**, 1989–1997, DOI: **10.1039/d1ra08890d**.
27 J. Gu, D. Hu, W. Wang, Q. Zhang, Z. Meng, X. Jia and K. Xi, *Biosens. Bioelectron.*, 2015, **68**, 27–33, DOI: **10.1016/j.bios.2014.12.027**.

28 R. Kaimal, V. Vinoth, A. S. Salunke, H. Valdes, R. V. Mangalaraja, B. Aljafri and S. Anandan, *Ultrason. Sonochem.*, 2022, **82**, 105868, DOI: 10.1016/j.ultsonch.2021.105868.
29 C. Liang, X. Xie, D. Zhang, J. Feng, S. Lu and Q. Shi, *J. Mater. Chem. B*, 2021, **9**, 5670–5681, DOI: 10.1039/d0tb02979c.
30 L. C. Sim, L. J. Yet, K. H. Leong, Y. K. Chinb and P. Saravanan, *Int. J. Biomass Renewables*, 2019, **8**, 9–16.
31 D. A. Gupta, M. L. Desai, N. I. Malek and S. K. Kailasa, *J. Mol. Struct.*, 2020, **1216**, 128343, DOI: 10.1016/j.molstruc.2020.128343.
32 G. A. Crosby and J. N. Demasa, *J. Phys. Chem. A*, 1971, **75**, 991, DOI: 10.1021/j100678a001.
33 J. R. Lakowicz, *Principles of Fluorescence Spectroscopy*, Springer, Boston, 2006, DOI: 10.1007/978-0-387-46312-4.
34 L. C. Ching, L. J. Yet, K. H. Leong, Y. H. Chinb and P. Saravanan, *Int. J. Biomass Renewables*, 2019, **8**(2), 9–16.
35 R. Atchudan, T. N. Nesakumar, K. R. Aseer, S. Perumal, N. Karthik and Y. R. Lee, *Biosens. Bioelectron.*, 2018, **99**, 303–311, DOI: 10.1016/j.bios.2017.07.076.
36 O. Akhavan, *Carbon*, 2014, **81**(1), 158–166, DOI: 10.1016/j.carbon.2014.09.044.
37 S. Thambiraj and D. R. Shankaran, *Appl. Surf. Sci.*, 2016, **390**, 435–443, DOI: 10.1016/j.apsusc.2016.08.106.
38 A. Kundu, B. Maity and S. Basu, *ACS Biomater. Sci. Eng.*, 2022, **8**, 4764–4776, DOI: 10.1021/acsbiomaterials.2c00798.
39 N. Sohal, S. Basu and B. Maity, *Microchem. J.*, 2023, **185**, 108287, DOI: 10.1016/j.microc.2022.108287.
40 W. Sun, S. Yang, Y. Liu, C. Shi, W. Shi, X. Lin, F. Guo and Y. Hong, *J. Phys. Chem. Solids*, 2021, **159**, 110283, DOI: 10.1016/j.jpcs.2021.110283.
41 S. Vandarkuzhali, V. Jeyalakshmi, G. Sivaraman, S. Singaravadivel, K. Krishnamurthy and B. Viswanathan, *Sens. Actuators, B*, 2017, **252**, 894–900, DOI: 10.1016/j.snb.2017.06.088.
42 Y. Liu, C. Zhu, Y. Gao, L. Yang, J. Xu, X. Zhang, C. Lu, Y. Wang and Y. Zhu, *Appl. Surf. Sci.*, 2020, **510**, 145437, DOI: 10.1016/j.apsusc.2020.145437.
43 A. Rosma and M. W. Cheong, *Malays. J. Microbiol.*, 2007, **3**, 19–26, DOI: 10.21161/mjm.00307.
44 L. Wang, Y. Bi, J. Hou, H. Li, Y. Xu, B. Wang, H. Ding and L. Ding, *Talanta*, 2016, **160**, 268–275, DOI: 10.1016/j.talanta.2016.07.020.
45 R. Bandi, B. R. Gangapuram, R. Dadigala, R. Eslavath, S. S. Singh and V. Guttena, *RSC Adv.*, 2016, **6**(34), 28633–28639, DOI: 10.1039/c6ra01669c.
46 S. Sahu, B. Behera, T. K. Maiti and S. Mohapatra, *Chem. Commun.*, 2012, **48**, 8835–8837, DOI: 10.1039/c2cc33796g.
47 H. Ding, S. B. Yu, J. S. Wei and H. M. Xiong, *ACS Nano*, 2016, **10**, 484–491, DOI: 10.1021/acsnano.5b05406.
48 J. Xu, S. Sahu, L. Cao, C. E. Bunker, G. Peng, Y. Liu, K. A. Fernando, P. Wang, E. A. Guliants, M. J. Meziani, H. Qian and Y. P. Sun, *Langmuir*, 2012, **28**, 16141–16147, DOI: 10.1021/la302506e.
49 V. Strauss, J. T. Margraf, C. Dolle, B. Butz, T. J. Nacken, J. Walter, W. Bauer, W. Peukert, E. Spiecker, T. Clark and D. M. Guldi, *J. Am. Chem. Soc.*, 2014, **136**, 17308–17316, DOI: 10.1021/ja510183c.
50 S. Zhu, J. Zhang, C. Qiao, S. Tang, Y. Li, W. Yuan, B. Li, L. Tian, F. Liu, R. Hu, H. Gao, H. Wei, H. Zhang, H. Sun and B. Yang, *Chem. Commun.*, 2011, **47**, 6858–6860, DOI: 10.1039/c1cc11122a.
51 V. N. Mochalin and Y. Gogotsi, *J. Am. Chem. Soc.*, 2009, **131**, 4594–4595, DOI: 10.1021/ja9004514.
52 N. Dhenadhayalan, K. C. Lin, R. Suresh and P. Ramamurthy, *J. Phys. Chem. C*, 2016, **120**, 1252–1261, DOI: 10.1021/acs.jpcc.5b08516.
53 P. D, S. Saini, A. Thakur, B. Kumar, S. Tyagi and M. K. Nayak, *J. Hazard. Mater.*, 2017, **328**, 117–126, DOI: 10.1016/j.jhazmat.2017.01.015.
54 S. Kainth, B. Maity and S. Basu, *RSC Adv.*, 2020, **10**(60), 36253–36264, DOI: 10.1039/d0ra06512a.
55 H. Huang, L. Liao, X. Xu, M. Zou, F. Liu and N. Li, *Talanta*, 2013, **117**, 152–157, DOI: 10.1016/j.talanta.2013.08.055.
56 F. Wang, Z. Gu, W. Lei, W. Wang, X. Xia and Q. Hao, *Sens. Actuators, B*, 2014, **190**, 516–522, DOI: 10.1016/j.snb.2013.09.009.
57 A. K. Singh, V. K. Singh, M. Singh, P. Singh, S. R. Khadim, U. Singh, B. Koch, S. H. Hasan and R. K. Asthana, *J. Photochem. Photobiol., A*, 2019, **376**, 63–72, DOI: 10.1016/j.jphotochem.2019.02.023.
58 F. Zhao, J. Qian, F. Quan, C. Wu, Y. Zheng and L. Zhou, *RSC Adv.*, 2017, **7**(70), 44178–44185, DOI: 10.1039/c7ra08097b.
59 P. Chen, J. Peng, Z. Zhang, X. Wang, X. Zhu, K. Fan and P. Luo, *Anal. Chim. Acta*, 2022, **1228**, 340341, DOI: 10.1016/j.aca.2022.340341.
60 F. Du, G. Li, X. Gong, G. Zhonghui, S. Shuang, M. Xian and C. Dong, *Sens. Actuators, B*, 2018, **277**, 492–501, DOI: 10.1016/j.snb.2018.09.027.
61 X. Gong, Z. Li, Q. Hu, R. Zhou, S. Shuang and C. Dong, *ACS Appl. Mater. Interfaces*, 2017, **9**(44), 38761–38772, DOI: 10.1021/acsami.7b11170.
62 S. Jayaweera, K. Yin, X. Hu and W. J. Ng, *Fluoresc*, 2019, **29**(6), 1291–1300, DOI: 10.1007/s10895-019-02452-7.
63 A. Mohammed, Y. Gugulothu, R. Bandi, R. Dadigala and U. K. Utkoor, *J. Chin. Chem. Soc.*, 2021, **68**(8), 1514–1521, DOI: 10.1002/jccs.202000545.
64 H. A. Benesi and J. H. Hildebrand, *J. Am. Chem. Soc.*, 1949, **71**, 2073–2707, DOI: 10.1021/ja01176a030.
65 S. Kainth, N. Goel, S. Basu and B. Maity, *New J. Chem.*, 2022, **46**(2), 686–694, DOI: 10.1039/d1nj04838d.
66 H. Qi, D. Huang, J. Jing, M. Ran, T. Jing, M. Zhao, C. Zhang, X. Sun, R. Sami and N. Benajiba, *RSC Adv.*, 2022, **12**(12), 7574–7583, DOI: 10.1039/d2ra00134a.
67 A. Kundu, B. Maity and S. Basu, *New J. Chem.*, 2022, **46**, 7545–7556, DOI: 10.1039/D2NJ00220E.
68 L. Liu, S. Anwar, H. Ding, M. Xu, Q. Yin, Y. Xiao, X. Yang, M. Yan and H. Bi, *J. Electroanal. Chem.*, 2019, **840**, 84–92, DOI: 10.1016/j.jelechem.2019.03.071.
69 W. Zheng, H. Wu, Y. Jiang, J. Xu, X. Li, W. Zhang and F. Qiu, *Anal. Biochem.*, 2018, **555**, 42–49, DOI: 10.1016/j.ab.2018.06.004.

70 Y. Wang, M. Feng, B. He, X. Chen, J. Zeng and J. Sun, *Appl. Surf. Sci.*, 2022, **599**, 153705, DOI: **10.1016/j.apsusc.2022.153705**.
71 J. Gu, D. Hu, W. Wang, Q. Zhang, Z. Meng, X. Jia and K. Xi, *Biosens. Bioelectron.*, 2015, **68**, 27–33, DOI: **10.1016/j.bios.2014.12.027**.
72 J. Ju, R. Zhang, S. He and W. Chen, *RSC Adv.*, 2014, **4**, 52583–52589, DOI: **10.1039/c4ra10601f**.
73 W. Dong, R. Wang, X. Gong and C. Dong, *Anal. Bioanal. Chem.*, 2019, **411**, 6687–6695, DOI: **10.1007/s00216-019-02042-3**.